Comparative Evaluation of ^{18}F-Labeled Glutamic Acid and Glutamine as Tumor Metabolic Imaging Agents

Karl Ploessl[1], Limin Wang[1], Brian P. Lieberman[1], Wenchao Qu[1], and Hank F. Kung[1,2]

[1]*Department of Radiology, University of Pennsylvania, Philadelphia, Pennsylvania; and* [2]*Department of Pharmacology, University of Pennsylvania, Philadelphia, Pennsylvania*

^{18}F-labeled (2*S*,4*R*)-4-fluoro-L-glutamine (4F-GLN) has demonstrated high uptake in tumor cells that undergo high growth and proliferation. Similar tumor targeting properties have also been observed for ^{18}F-labeled (2*S*,4*R*)-4-fluoro-L-glutamate (4F-GLU), suggesting that both are useful imaging agents. A new labeling procedure facilitates the preparation of ^{18}F-(2*S*,4*R*)4F-GLN and ^{18}F-(2*S*,4*R*)4F-GLU with confirmed radiochemical and enantiomeric purity. Here, we report the preparation and comparative evaluation of ^{18}F-(2*S*,4*R*)4F-GLN and ^{18}F-(2*S*,4*R*)4F-GLU as tumor metabolic imaging agents. **Methods:** Uptake of enantiomerically pure ^{18}F-(2*S*,4*R*)4F-GLN and ^{18}F-(2*S*,4*R*)4F-GLU was determined in 3 tumor cell lines (9L, SF188, and PC-3) at selected time points. The in vitro cell uptake mechanism was evaluated by inhibition studies in 9L cells. In vivo biodistribution and PET studies were performed on male F344 rats bearing 9L tumor xenografts. **Results**: In vitro cell uptake studies showed that ^{18}F-(2*S*,4*R*)4F-GLN displayed higher uptake than ^{18}F-(2*S*,4*R*)4F-GLU. Amino acid transport system ASC (alanine-serine-cysteine–preferring; in particular, its subtype ASCT2 [*SLC1A5* gene]) and system X_c^- (*SLC7A11* gene) played an important role in transporting ^{18}F-(2*S*,4*R*)4F-GLN and ^{18}F-(2*S*,4*R*)4F-GLU, respectively, across the membrane. After being transported into cells, a large percentage of ^{18}F-(2*S*,4*R*)4F-GLN was incorporated into protein, whereas ^{18}F-(2*S*,4*R*)4F-GLU mainly remained as the free amino acid in its original form. In vivo studies of ^{18}F-(2*S*,4*R*)4F-GLN in the 9L tumor model showed a higher tumor uptake than ^{18}F-(2*S*,4*R*)4F-GLU, whereas ^{18}F-(2*S*,4*R*)4F-GLU had a slightly higher tumor-to-background ratio than ^{18}F-(2*S*,4*R*)4F-GLN. Imaging studies showed that both tracers had fast accumulation in 9L tumors. Compared with ^{18}F-(2*S*,4*R*)4F-GLU, ^{18}F-(2*S*,4*R*)4F-GLN exhibited prolonged tumor retention reflecting its incorporation into intracellular macromolecules. **Conclusion:** Differences in uptake and metabolism in tumor cells were found between ^{18}F-(2*S*,4*R*)4F-GLN and ^{18}F-(2*S*,4*R*)4F-GLU. Both agents are potentially useful as metabolic tracers for tumor imaging.

Key Words: ^{18}F; PET; tumor imaging; glutamine; glutamic acid/glutamate

J Nucl Med 2012; 53:1616–1624
DOI: 10.2967/jnumed.111.101279

Many ^{11}C- and ^{18}F-labeled amino acids, such as L-^{11}C-methionine (*1*), *O*-(2-^{18}F-fluoroethyl)-tyrosine (^{18}F-FET) (*2*), 3-^{18}F-α-methyl-L-tyrosine (*3*), 6-^{18}F-fluoro-L-dopa, 3-*O*-methyl-6-^{18}F-fluoro-L-dopa, and *anti*-1-amino-3-^{18}F-fluorocyclobutyl-carboxylic acid (*anti*-^{18}F-FACBC), have been used as PET tumor imaging agents in humans (*4–7*). Uptake of labeled amino acids in tumor cells is associated mostly with increased expression of amino acid transporters, particularly system L (leucine-preferring) and system ASC (alanine-serine-cysteine–preferring). PET with these amino acid–based tracers shows promise as a tool for the diagnosis and staging of human cancers (*4*). ^{18}F-FET, a tyrosine analog, is transported across the cell membrane via system L. It does not incorporate into cellular proteins. In contrast to ^{18}F-FDG and methionine, ^{18}F-FET is not taken up in inflammatory cells. As such, it is often used for imaging brain tumors, such as gliomas, to distinguish between tumor growth and local inflammation (*2*). Additionally, there is evidence that ^{18}F-FET may distinguish recurrent tumor from post-therapy effects, although ^{18}F-FET uptake can occur in reactive astrocytes (*8*). Another clinically used nonnatural amino acid *anti*-^{18}F-FACBC, a leucine analog, is transported via systems L and ASC. Recent human studies of *anti*-^{18}F-FACBC suggest that it is a useful imaging agent for prostate tumors (*9–11*).

Upregulation of glycolysis in tumor tissue has enabled ^{18}F-FDG PET tumor imaging. However, a significant number of malignant tumors are ^{18}F-FDG PET–negative. Recent studies suggested that several tumors may use glutamine as the key nutrient for survival (*12–16*) and that ^{18}F-FDG–negative tumors may use a different metabolic pathway—"glutaminolysis" (*17–22*). Currently, most reported amino acid–based PET agents are designed to target the increase of amino acid transporters. However, since they are not structurally related to glutamine, they are unlikely to be specific for increases in glutamine metabolism (glutaminolysis) in tumors (*20,22,23*). As an alternative metabolic tracer for tumors, ^{18}F-(2*S,4R*)4-fluoroglutamine (^{18}F-(2*S*,4*R*)4F-GLN) was developed as a PET tracer for mapping glutaminolytic tumors. The results showed that ^{18}F-(2*S*,4*R*)4F-GLN is selectively taken up and trapped by tumor cells. It may be useful as a novel metabolic tracer for tumor imaging (*24*).

Received Nov. 24, 2011; revision accepted May 2, 2012.
For correspondence or reprints contact: Hank F. Kung, Department of Radiology, University of Pennsylvania, 3700 Market St., Room 305, Philadelphia, PA 19104.
E-mail: kunghf@gmail.com
Published online Aug. 30, 2012.

Recently, a report on using a new ^{18}F-labeled glutamic acid, (4*S*)-4-(3-^{18}F-fluoropropyl)-L-glutamate (Bayer ligand BAY 94-9392), for tumor imaging has highlighted the importance of alternative amino acid derivatives in detecting tumor proliferation. This ^{18}F-labeled glutamic acid derivative showed good tumor uptake in animal models and humans (*25,26*). Tracer uptake studies and analysis of knockdown cells showed specific transport of BAY 94-9392 via the cystine/glutamate exchanger designated as system X_c^- (*SLC7A11* gene). No metabolites were observed in mouse blood and tumor cells. PET with excellent tumor visualization and high tumor-to-background ratios was achieved in preclinical tumor models. In addition, BAY 94-9392 did not accumulate in inflammatory lesions, in contrast to ^{18}F-FDG (*26*). Therefore, BAY 94-9392 may be useful to examine system X_c^- (*SLC7A11*) activity in vivo as a possible hallmark of tumor oxidative stress. Another Bayer ligand, 4-^{18}F-fluoroglutamic acid (BAY 85-8050), exhibited rapid tumor uptake in lung and colon cancer cells (*25*). But BAY 85-8050 was a diastereomeric mixture of ^{18}F-(2*S*,4*S*) and (2*S*,4*R*)-fluoroglutamate (^{18}F-glutamic acid). The tumor uptakes are highly stereoselective, and this situation complicates the analysis of biologic data of BAY 85-8050.

Although ^{18}F-(2*S*,4*R*)4F-GLN is taken up into tumors via upregulation of glutamine use in tumor cells, the potential usefulness of the corresponding ^{18}F-(2*S*,4*R*)4F-GLU has not been fully investigated. We reasoned that ^{18}F-(2*S*,4*R*)4F-GLU may also be taken up by tumor tissues as reported for ^{18}F-(2*S*,4*R*)4F-GLU derivatives. Reported here is the preparation and biologic evaluation of enantiomerically pure ^{18}F-(2*S*,4*R*)4F-GLN and ^{18}F-(2*S*,4*R*)4F-GLU.

MATERIALS AND METHODS

Synthesis of ^{18}F-(2*S*,4*R*)4F-GLN and ^{18}F-(2*S*,4*R*)4F-GLU

Synthesis of the labeling precursor and radiolabeling of ^{18}F-(2*S*,4*R*)4F-GLN were described before (*23,24*). Preparation of ^{18}F-(2*S*,4*R*)4F-GLU followed the same reported procedure except that at the deprotection reaction, 6N HCl (at 100°C) was used instead of trifluoroacetic acid (at 60°C). The hydrochloric acid hydrolysis selectively led to the desired glutamic acid, ^{18}F-(2*S*,4*R*)4F-GLU (Scheme 1).

Cell Culture

9L (ATCC), SF188 (Neurosurgery Tissue Core, University of California, San Francisco), and PC-3 (ATCC) cell lines were cultured according to ATCC recommendation, in Dulbecco modified Eagle medium (Gibco BRL) and F-12K medium, respectively, supplemented with 10% fetal bovine serum (Hycolne) and 1% penicillin/streptomycin. Cells were maintained in a T-75 culture flask under humidified incubator conditions (37°C, 5% CO_2) and were routinely passaged at confluence.

Cell Uptake Assay

Tumor cells were plated in culturing medium 24 h before studies. On the day of the experiments, the medium was aspirated

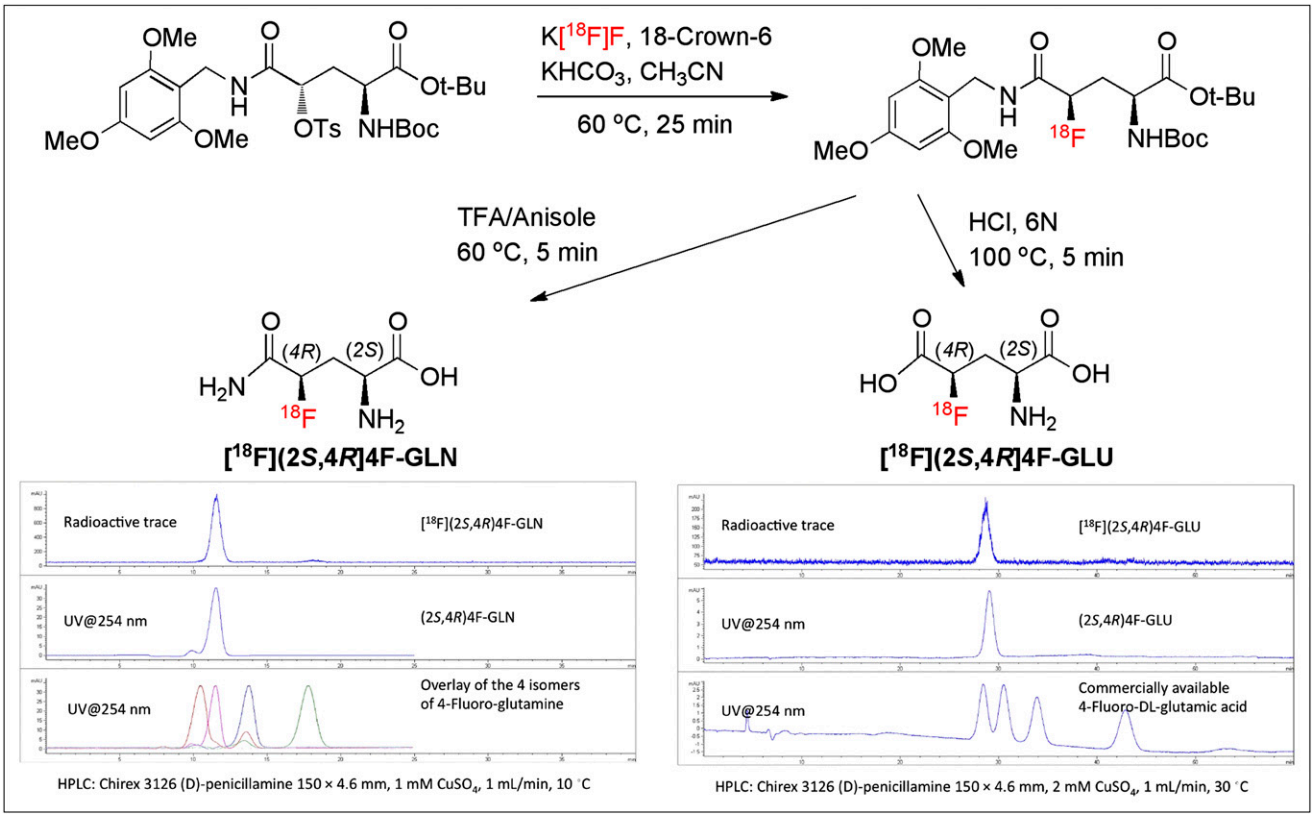

SCHEME 1. Radiosynthesis and identification of ^{18}F-(2*S*,4*R*)4F-GLN and ^{18}F-(2*S*,4*R*)4F-GLU. HPLC = high-performance liquid chromatography; TFA = trifluoroacetic acid; UV = ultraviolet.

and the cells were washed 3 times with phosphate-buffered saline (PBS, containing Ca^{2+} and Mg^{2+}). ^{18}F-(2*S*,4*R*)4F-GLU or ^{18}F-(2*S*,4*R*)4F-GLN was mixed with warm (37°C) PBS (with Ca^{2+} and Mg^{2+}) and was then added to each well (37 kBq/mL/well) together with ^{3}H-L-glutamine (^{3}H-GLN) (37 kBq/mL/well). The cells were incubated at 37°C for 5, 30, 60, and 120 min. At the end of the incubation period, the PBS solution containing the ligands was aspirated and the cells were washed 3 times with 1 mL of ice-cold PBS without Ca^{2+} and Mg^{2+}. After the washing with ice-cold PBS, 350 μL of 1N NaOH were used to lyse the cells. The lysed cells were collected onto filter paper and counted together with samples of the initial dose using a γ-counter (Packard Cobra). One hundred microliters of the cell lysate were used for determination of the protein concentration by a modified Lowry protein assay. The data were normalized as percentage uptake of initial dose relative to 100 μg of protein content.

Transport Characterization Studies

In competitive inhibition experiments, uptake of ^{18}F-(2*S*,4*R*)4F-GLU and ^{18}F-(2*S*,4*R*)4F-GLN in 9L cells was measured in the presence of specific inhibitors (for systems A, ASC, L, N, X_c^- [*SLC7A11*], and X_{AG}^- p*SLC1A1*]) in a range of concentrations from 0.1 to 5 mM in PBS solution. In sodium-dependence studies, PBS buffer was replaced with Na^+-free solution (143 mM choline chloride, 2.68 mM KCl, and 1.47 mM KH_2PO_4). In pH-dependence studies, PBS solution was adjusted to a desirable pH with NaOH and HCl solution. The cells were incubated at 37°C for 60 min. The procedure for incubation was the same as in cell uptake studies. The data were normalized in reference to uptake of ^{18}F-(2*S*,4*R*)4F-GLU or ^{18}F-(2*S*,4*R*)4F-GLN without any inhibitor in PBS solution at pH 7.4.

Protein Incorporation

To measure the extent of protein incorporation of the tracers, protein-bound activity in SF188 and 9L cells was determined at 30 and 120 min after incubation. The cells were incubated with 222 kBq of ^{18}F-(2*S*,4*R*)4F-GLU or ^{18}F-(2*S*,4*R*)4F-GLN together with 37 kBq of ^{3}H-GLN in 3 mL of PBS. At the end of incubation, radioactive medium was removed and the cells were washed 3 times with ice-cold PBS without Ca^{2+} and Mg^{2+}, treated with 0.25% trypsin, and resuspended in PBS. The samples were centrifuged (13,000 rpm, 5 min), the supernatant removed, and the cells suspended in 200 μL of 1% Triton-X 100 (Sigma). After vortex mixing, 800 μL of ice-cold 15% trichloroacetic acid (TCA) were added to the solution. After 30 min of precipitation, the cells were centrifuged again (13,000 rpm, 15 min) and washed twice with 15% ice-cold TCA. The radioactivity in supernatant and pellet was determined. Protein incorporation was calculated as percentage of acid-precipitable activity. The method was validated by incubating cells in the medium containing 5 μg of cycloheximide per milliliter under otherwise identical incubation and workup conditions.

In Vivo Biodistribution Study in Fischer 344 Rats Bearing 9L Tumors

Fischer 344 rats were purchased from Charles River Laboratories. Cells were resuspended in PBS (containing 0.90 mM Ca^{2+} and 1.05 mM Mg^{2+}). Xenografts consisting of 8–10 million 9L cells were injected subcutaneously (0.2 mL) into the right shoulder flank of each Fischer 344 rat. Proliferation of cells took 12–15 d to reach an appropriate tumor size (1-cm diameter). Three to six rats per group were used for the biodistribution study. All animals were kept fasting for 12–18 h before the study (this procedure follows our laboratory protocol and follows the clinical protocol for ^{18}F-FDG PET (*27*)). The rats were then put under anesthesia with isoflurane (2%–3%), and 0.20 mL of saline solution containing 925 kBq (25 μCi) of activity was injected intravenously. The rats were sacrificed at selected time points after injection by cardiac excision while under isoflurane anesthesia. The organs of interest were removed and weighed, and the radioactivity was counted with a γ-counter (Packard Cobra). The percentage dose per gram was calculated by a comparison of the tissue activity counts to counts of 1.0% of the initial dose. Results were expressed as the percentage of the injected dose per gram of tissue. Each value represents the mean ± SD of 6 rats unless otherwise noted.

Dynamic small-animal PET studies were conducted on Fisher rats bearing 9L xenografts using a Mosaic small-animal PET scanner (Phillips). Under isoflurane anesthesia (1%–2%, 1 L of oxygen per minute), the tumor-bearing F344 rats as described before were injected (intravenously) with 19–37 MBq (0.5–1.0 mCi) of activity. Dynamic scans were conducted over a period of 2 h (5 min/frame; image voxel size, 0.5 mm^3). Images were reconstructed, and region-of-interest analysis was performed using AMIDE software (http://amide.sourceforge.net/).

RESULTS

Radiosynthesis of ^{18}F-(2*S*,4*R*)4F-GLN and ^{18}F-(2*S*,4*R*)4F-GLU

Radiosynthesis of optically pure ^{18}F-(2*S*,4*R*)4F-GLN followed the reported procedure (*23*). Preparation of ^{18}F-(2*S*,4*R*)4F-GLU used the same method except that in the deprotection reaction 6N HCl (at 100°C) was used instead of trifluoroacetic acid (at 60°C). Both tracers were prepared with high radiochemical and optical purity (>95%) (Scheme 1). The identity and purity of the 2 tracers was established by comparing them with cold (2*S*,4*R*)4F-GLN and (2*S*,4*R*)4F-GLU, respectively, and in the case of ^{18}F-(2*S*,4*R*)4F-GLU additionally with commercially available 4-fluoro-DL-glutamic acid (AlfaAesar) on chiral high-performance liquid chromatography.

In Vitro Cell Uptake Studies

Time-dependent uptake of ^{18}F-(2*S*,4*R*)4F-GLN and ^{18}F-(2*S*,4*R*)4F-GLU in PBS was determined in rat glioma 9L cells, human glioblastoma SF188 cells, and prostate cancer PC-3 cells, using ^{3}H-GLN as an internal reference ligand. As represented in 9L cells (Fig. 1), ^{18}F-(2*S*,4*R*)4F-GLN had high and linearly increasing uptake over a 120-min period in contrast to ^{3}H-GLN, which reached maximum uptake in 30 min and then washed out. Uptake of ^{18}F-(2*S*,4*R*)4F-GLU had an incremental increase as well, but much slower than ^{18}F-(2*S*,4*R*)4F-GLN. Uptake of ^{18}F-(2*S*,4*R*)4F-GLN at selected time points was 1.5- to 5.6-fold higher than that of ^{18}F-(2*S*,4*R*)4F-GLU (Table 1). We examined the uptake of ^{18}F-(2*S*,4*R*)4F-GLN in PBS containing different concentrations of glucose from 0.1 to 5 mM at 60 min. The result showed that glucose did not have a significant impact on uptake of ^{18}F-(2*S*,4*R*)4F-GLN. When we used as a control the uptake of ^{18}F-(2*S*,4*R*)4F-GLN in PBS without glucose, the uptake in PBS containing 5 mM glucose was 102.1 ± 6.94% that of the control.

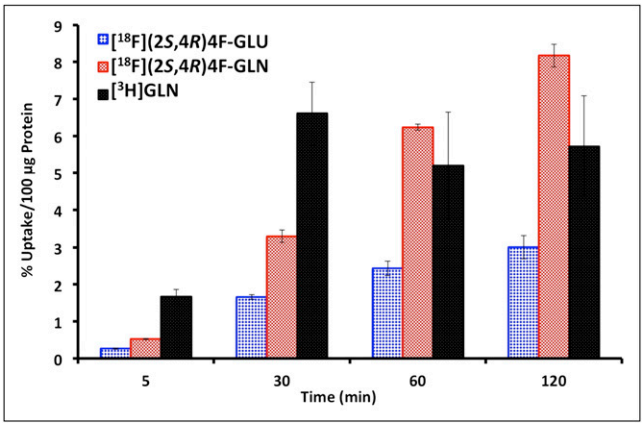

FIGURE 1. Time-dependent uptake of ^{18}F-(2*S*,4*R*)4F-GLU, ^{18}F-(2*S*,4*R*)4F-GLN, and ^{3}H-GLN in PBS in 9L cells. Data are expressed as percentage of uptake in 100 μg of protein (mean ± SD, $n = 3$) (1-way ANOVA for cell uptake studies in 9L cells: 5 min, $P < 0.001$; 30 min, $P < 0.001$; 60 min, $P = 0.004$; 120 min, $P = 0.001$). GLN = glutamine; GLU = glutamic acid.

Transport Characterization Studies in 9L Glioma

We investigated the potential transport mechanisms involved in the uptake of ^{18}F-(2*S*,4*R*)4F-GLU and ^{18}F-(2*S*,4*R*)4F-GLN in 9L cells via a series of competitive inhibition studies, ion-dependence studies, and pH-dependence studies. The result of inhibition studies showed that system A inhibitor MeAIB ([*N*-methyl]-α-methylaminoisobutyric acid) had no inhibitory effect on the uptake of either ^{18}F-(2*S*,4*R*)4F-GLU or ^{18}F-(2*S*,4*R*)4F-GLN. System L inhibitor BCH (2-aminobicyclo[2.2.1]heptane-2-carboxylic acid), system ASC inhibitor L-serine, and system ASC N inhibitor L-glutamine (L-GLN) exhibited a similar concentration-dependent reduction of uptake of ^{18}F-(2*S*,4*R*)4F-GLN while showing no apparent inhibitory effect on ^{18}F-(2*S*,4*R*)4F-GLU uptake (Fig. 2). This indicates that systems L, ASC, and N might contribute to the uptake of ^{18}F-(2*S*,4*R*)4F-GLN but not to the transport of ^{18}F-(2*S*,4*R*)4F-GLU.

The ion-dependence studies demonstrated that transport of both ^{18}F-(2*S*,4*R*)4F-GLU and ^{18}F-(2*S*,4*R*)4F-GLN was Na^+-dependent. In Na^+-free medium, their uptake was reduced to approximately 20% of the control (Fig. 2). ^{18}F-(2*S*,4*R*)4F-GLN was insensitive to a change in pH from 6 to 8, whereas ^{18}F-(2*S*,4*R*)4F-GLU uptake was reduced to approximately 70% of the control in acidic medium (pH 6).

TABLE 1
Ratios of ^{18}F-(2*S*,4*R*)4F-GLN* Uptake to ^{18}F-(2*S*,4*R*)4F-GLU Uptake in Different Tumor Cell Lines

Time (min)	9L	SF188	PC-3
5	1.52 ± 0.26	2.90 ± 0.85	5.56 ± 1.62
30	1.85 ± 0.35	2.57 ± 0.60	5.31 ± 1.60
60	2.59 ± 1.05	1.78 ± 0.51	4.23 ± 1.26
120	2.78 ± 1.02	1.47 ± 0.38	4.22 ± 0.55

*Data were first published by Lieberman et al. (*24*).

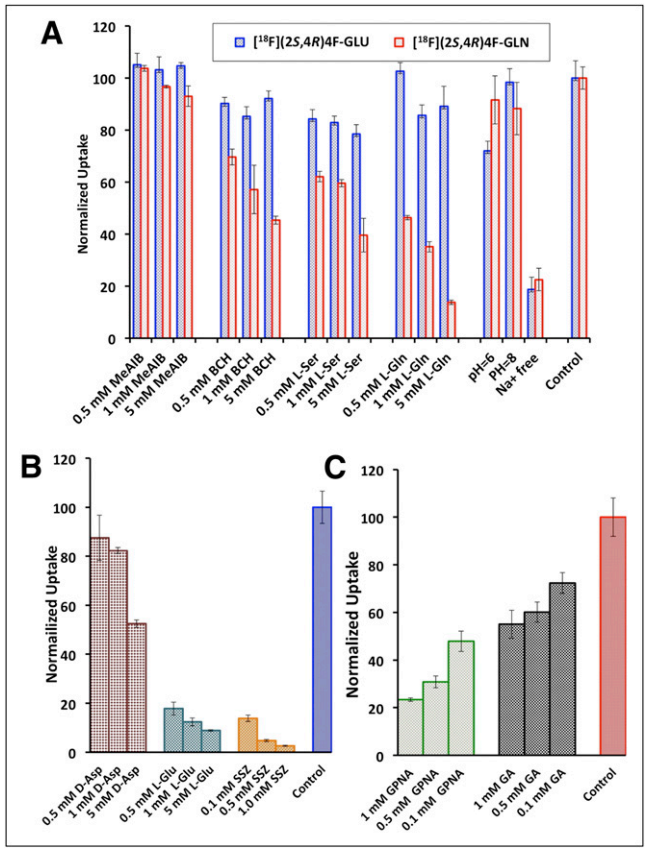

FIGURE 2. (A) Uptake of ^{18}F-(2*S*,4*R*)4F-GLN and ^{18}F-(2*S*,4*R*)4F-GLU in 9L cells in presence of inhibitors for systems A, ASC, L, and N and in medium free of Na^+ or at various pH levels. (B) Uptake of ^{18}F-(2*S*,4*R*)4F-GLU in presence of inhibitors for X_c^- (*SLC7A11*) and X_{AG}^- (*SLC1A1*). (C) Uptake of ^{18}F-(2*S*,4*R*)4F-GLN in presence of inhibitors for ASCT2 (*SLC1A5*). Uptake values are normalized to uptake of tracers in PBS in absence of inhibitors. Data are normalized uptake values (mean ± SD, $n = 3$). GLN = glutamine; GLU = glutamic acid.

Because the activity of system N is very pH-sensitive and is almost inactive at pH 6 (*28*), system N might not play an important role in the transport of ^{18}F-(2*S*,4*R*)4F-GLN. We also differentiated the roles of 2 subtypes of system ASC, ASCT1 (*SLC1A4*) and ASCT2 (*SLC1A5*), in the uptake of ^{18}F-(2*S*,4*R*)4F-GLN via comparison of the inhibitory effect of L-γ-glutamyl-*p*-nitroanilide, a potent ASCT2 (*SLC1A5*) inhibitor, to its close analog L-γ-glutamyl-anilide, which is inactive toward ASCT2 (*SLC1A5*) (Fig. 2). L-γ-glutamyl-*p*-nitroanilide had a greater impact on the uptake: 1 mM L-γ-glutamyl-*p*-nitroanilide could reduce the uptake by 77%, compared with 44% when 1 mM L-γ-glutamyl-anilide was present. The results of these studies suggest that the transport of ^{18}F-(2*S*,4*R*)4F-GLN might involve both sodium-independent system L and sodium-dependent system ASC, with preference to its subtype ASCT2 (*SLC1A5*).

Uptake of ^{18}F-(2*S*,4*R*)4F-GLU was strongly inhibited by sulfasalazine or L-glutamic acid (L-GLU), inhibitors for X_c^- (*SLC7A11*) (Fig. 2) (*29*). D-aspartic acid, a specific inhibitor for X_{AG}^-, also had some inhibitory effect, but not as potent as sulfasalazine or L-GLU (*30*). The uptake

of ^{18}F-(2*S*,4*R*)4F-GLU was reduced to less than 10% of the control by the presence of 5 mM X_c^- (*SLC7A11*) inhibitors, in contrast to 50% by X_{AG}^- inhibitor. These results indicate that both Na^+-dependent X_{AG}^- (*SLC1A1*) and Na^+-independent X_c^- (*SLC7A11*) systems were involved in the transport of ^{18}F-(2*S*,4*R*)4F-GLU, with X_c^- (*SLC7A11*) possibly playing a more dominant role.

Protein Incorporation

Incorporation of ^{18}F-(2*S*,4*R*)4F-GLN and ^{18}F-(2*S*,4*R*)4F-GLU into protein at 30 and 120 min in 9L and SF188 cell lines was measured using ^{3}H-GLN as the reference ligand (Fig. 3). ^{18}F-(2*S*,4*R*)4F-GLN and ^{3}H-GLN exhibited a similar protein incorporation profile. A large percentage of ^{18}F-(2*S*,4*R*)4F-GLN incorporated into protein after 2 h. At 30 and 120 min, the protein incorporation of ^{18}F-(2*S*,4*R*)4F-GLN in 9L cells was 29% and 72%, respectively, and in SF188 cells, 12% and 62%, respectively. In contrast, ^{18}F-(2*S*,4*R*)4F-GLU had negligible incorporation into protein; most of the activity remained in the TCA-soluble fraction. To validate the methodology, SF188 cells were incubated in a medium containing a 5 μg/mL concentration of cycloheximide (a known inhibitor of protein biosynthesis in eukaryotic organisms). Under these conditions, incorporation at 120 min of ^{3}H-GLN, ^{18}F-(2*S*,4*R*)4F-GLN, and ^{18}F-(2*S*,4*R*)4F-GLU was reduced to 13%, 9%, and 1%, respectively.

In Vivo Biodistribution Studies in Rats Bearing 9L Xenografts

The in vivo biodistribution studies of ^{18}F-(2*S*,4*R*)4F-GLU and ^{18}F-(2*S*,4*R*)4F-GLN were performed on Fisher rats bearing 9L xenografts. The distribution of radioactivity in tissues after intravenous injection of ^{18}F-(2*S*,4*R*)4F-GLU at selected time points is summarized in Figure 4. Rapid washout of radioactivity from blood, heart, lung, pancreas, spleen, and liver was observed. Apart from bone or bone marrow, other examined organs had continuously decreasing radioactivity after 15 min. Bone or bone marrow uptake increased as a function of time from 0.84 at 2 min to 1.86 at 120 min, indicating either substantial defluorination or bone marrow uptake. Tumor uptake of ^{18}F-(2*S*,4*R*)4F-GLU reached a maximum of 1.1 at around 15 min and then decreased. The highest uptake was in the kidney, suggesting that ^{18}F-(2*S*,4*R*)4F-GLU was excreted mainly through the urinary tract.

In comparison to ^{18}F-(2*S*,4*R*)4F-GLU at 30 and 60 min (Table 2), ^{18}F-(2*S*,4*R*)4F-GLN generally had higher uptake in the organs except in kidney and bone. In particular, ^{18}F-(2*S*,4*R*)4F-GLN had much higher uptake in the pancreas, similar to many naturally occurring amino acids. Tumor uptake of ^{18}F-(2*S*,4*R*)4F-GLN was 1.3- to 2.2-fold higher than that of ^{18}F-(2*S*,4*R*)4F-GLU at 30 and 60 min, respectively. Both tracers showed respectable tumor uptake compared with the surrounding tissues; their tumor-to-blood ratio was comparable. Although ^{18}F-(2*S*,4*R*)4F-GLN had higher tumor uptake, the tumor-to-muscle and tumor-to-brain ratios of ^{18}F-(2*S*,4*R*)4F-GLU were higher. The tumor-to-muscle ratio of ^{18}F-(2*S*,4*R*)4F-GLU increased from 6.36 at 30 min to 11.16 at 60 min. In contrast, the tumor-to-muscle ratio of ^{18}F-(2*S*,4*R*)4F-GLN decreased from 2.78 at 30 min to 2.00 at 60 min. Both tracers' tumor-to-brain ratio decreased from 30 to 60 min, 17.64 to 7.13 and 9.36 to 5.85 for ^{18}F-(2*S*,4*R*)4F-GLU and ^{18}F-(2*S*,4*R*)4F-GLN, respectively.

Small-Animal Imaging Studies

Dynamic small-animal PET studies were conducted with ^{18}F-(2*S*,4*R*)4F-GLU and ^{18}F-(2*S*,4*R*)4F-GLN on rats bearing 9L xenografts. One tumor per rat was injected. The tumors did not grow homogenously, and they had an elongated, non-

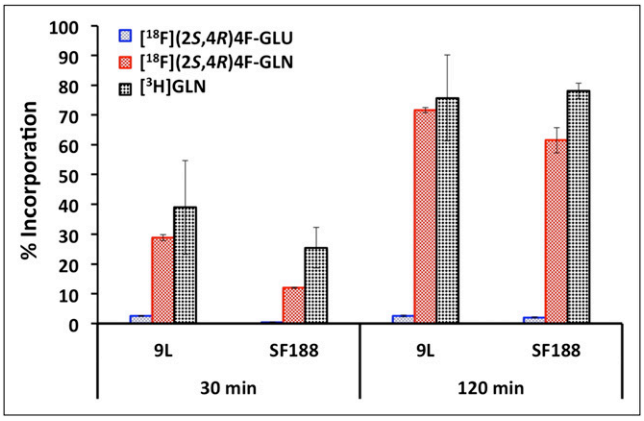

FIGURE 3. Protein incorporation of ^{18}F-(2*S*,4*R*)4F-GLN and ^{18}F-(2*S*,4*R*)4F-GLU in 9L and SF188 tumor cell lines. ^{3}H-GLN was used as reference ligand. Only glutamine ^{3}H-GLN and derivative ^{18}F-(2*S*,4*R*)4F-GLN showed significant cellular incorporation; corresponding glutamic acid derivative displayed low cell trapping. Data are percentage of TCA-insoluble fraction (% incorporation) (mean ± SD, n = 3–6) (1-way ANOVA for protein incorporation: in 9L cells, P = 0.007 [30 min], $P < 0.001$ [120 min]; in SF188 cells, P = 0.001 [30 min], $P < 0.001$ [120 min]). BCH = 2-aminobicyclo[2.2.1]heptane-2-carboxylic acid; D-Asp = D-aspartic acid; GA = L-γ-glutamyl-anilide; GLN = glutamine; GLU = glutamic acid; GPNA = L-γ-glutamyl-*p*-nitroanilide; L-Ser = L-serine; MeAIB = [*N*-methyl]-α-methylaminoisobutyric acid; SSZ = sulfasalazine.

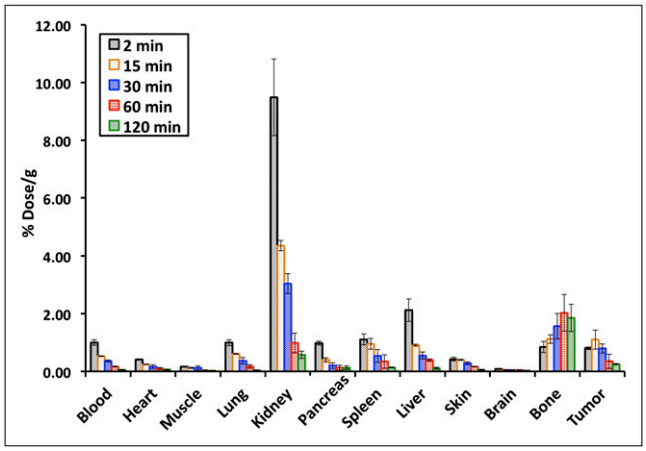

FIGURE 4. In vivo biodistribution study of ^{18}F-(2*S*,4*R*)4F-GLU in rats bearing 9L xenografts. Data are percentage initial dose per gram, mean ± SD (n = 3).

TABLE 2
Biodistribution Studies of ^{18}F-(2*S*,4*R*)4F-GLN and ^{18}F-(2*S*,4*R*)4F-GLU in Rats Bearing 9L Tumor After Intravenous Injection

Organ	30 min		60 min	
	^{18}F-(2*S*,4*R*)4F-GLU	^{18}F-(2*S*,4*R*)4F-GLN*	^{18}F-(2*S*,4*R*)4F-GLU	^{18}F-(2*S*,4*R*)4F-GLN*
Blood	0.36 ± 0.03	0.43 ± 0.01	0.17 ± 0.02	0.32 ± 0.02
Heart	0.16 ± 0.07	0.36 ± 0.02	0.09 ± 0.04	0.35 ± 0.01
Muscle	0.12 ± 0.07	0.37 ± 0.02	0.03 ± 0.02	0.38 ± 0.03
Lung	0.37 ± 0.34	0.64 ± 0.02	0.17 ± 0.06	0.41 ± 0.04
Kidney	3.04 ± 0.02	1.02 ± 0.12	0.99 ± 0.34	0.76 ± 0.18
Pancreas	0.20 ± 0.10	2.14 ± 0.27	0.13 ± 0.09	1.36 ± 0.16
Spleen	0.53 ± 0.22	0.76 ± 0.05	0.34 ± 0.23	0.53 ± 0.04
Liver	0.55 ± 0.12	0.98 ± 0.15	0.39 ± 0.04	0.66 ± 0.13
Skin	0.28 ± 0.05	0.42 ± 0.11	0.16 ± 0.01	0.29 ± 0.04
Brain	0.05 ± 0.01	0.11 ± 0.01	0.05 ± 0.00	0.13 ± 0.00
Bone	1.57 ± 0.44	0.78 ± 0.13	2.03 ± 0.64	1.03 ± 0.38
9L tumor	0.79 ± 0.16	1.03 ± 0.14	0.35 ± 0.25	0.76 ± 0.21
Tumor/blood	2.18 ± 0.47	2.40 ± 0.33	2.11 ± 1.52	2.38 ± 0.67
Tumor/muscle	6.36 ± 3.92	2.78 ± 0.41	11.2 ± 10.9	2.00 ± 0.57
Tumor/brain	17.6 ± 5.02	9.36 ± 1.53	7.13 ± 5.09	5.85 ± 1.61

*Data were first published by Lieberman et al. (*24*).
Data are average percentage dose per gram, mean ± SD (*n* = 3 to 6).

uniform shape. Their representative 2-h summed images (Fig. 5) and time–activity curves (Figs. 6A and 6B) for assessing kinetics were generated by drawing regions of interest. Tumors could be visualized with both tracers. ^{18}F-(2*S*,4*R*)4F-GLN had higher tumor uptake and higher background than ^{18}F-(2*S*,4*R*)4F-GLU. There was apparent uptake in the skeleton in both images, indicating either defluorination or bone marrow uptake of the tracers. The time–activity curve from image analysis showed uptake of ^{18}F-(2*S*,4*R*)4F-GLU in tumor and muscle. It reached a maximum in 10–20 min and then declined quickly. ^{18}F-(2*S*,4*R*)4F-GLN had fast uptake in tumor and muscle as well, but the activity remained rather constant after reaching a maximum at around 20 min. Similar to the result of biodistribution studies, kinetic analysis showed that the tumor-to-muscle ratio of ^{18}F-(2*S*,4*R*)4F-GLU was slightly higher than that of ^{18}F-(2*S*,4*R*)4F-GLN (Fig. 6C). Brain uptake was low for both ^{18}F-(2*S*,4*R*)4F-GLN and ^{18}F-(2*S*,4*R*)4F-GLU. The tracer also showed uptake in the lymph nodes, and additional studies will be needed in the future.

DISCUSSION

Cellular metabolic changes provide the basis for tumor diagnostic and therapeutic monitoring. The most prominent example is ^{18}F-FDG PET, which detects the high rate of glycolysis in tumor cells (*31*). Growing evidence suggests that certain amino acids play important roles in tumor growth and proliferation (*32*). In particular, glutamine and glutamate have received special attention resulting from emerging evidence that the reprogrammed tumor metabolism

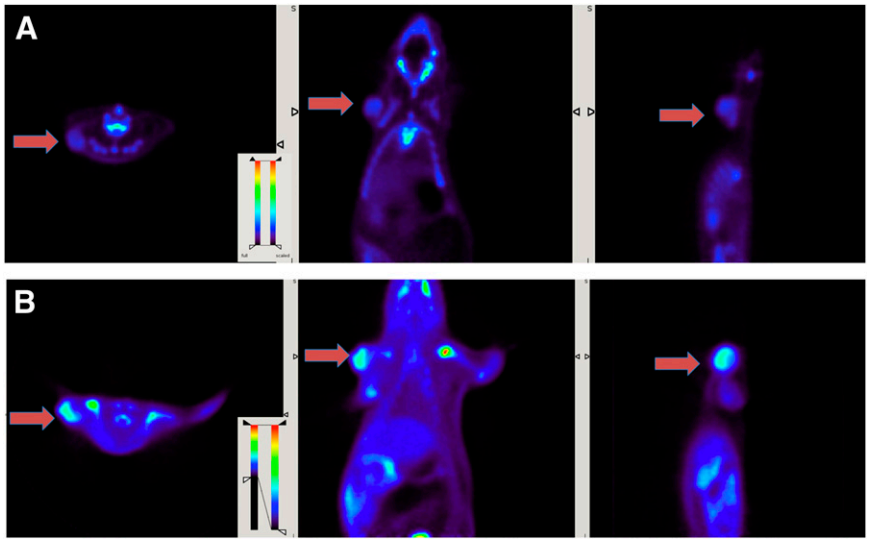

FIGURE 5. Summed 120-min small-animal PET images of ^{18}F-(2*S*,4*R*)4F-GLU (A) and ^{18}F-(2*S*,4*R*)4F-GLN (B) in rats bearing 9L tumor model. Data represent summed 2-h scan from transverse, coronal, and sagittal views (left to right). Arrows indicate location of 9L tumors.

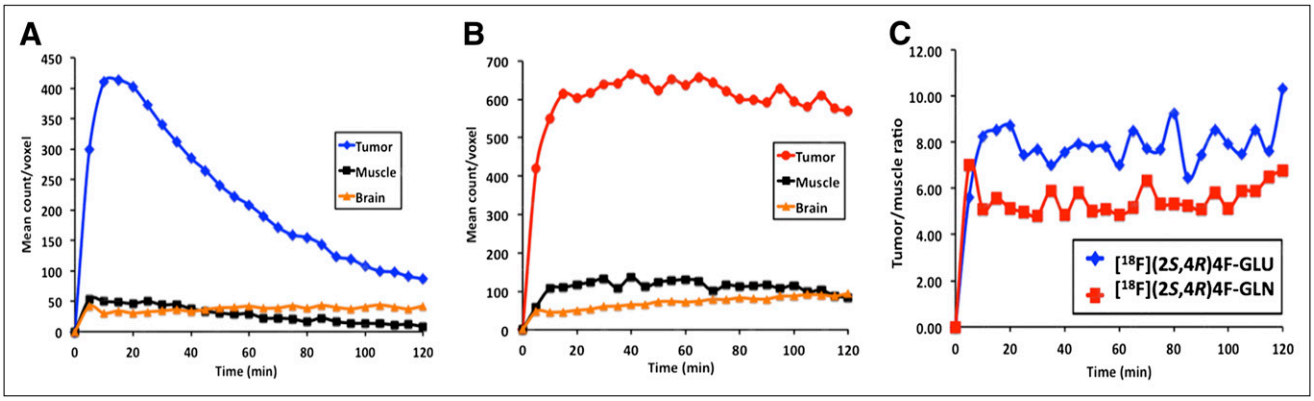

FIGURE 6. (A) Time–activity curve of ^{18}F-(2*S*,4*R*)4F-GLU in rats bearing 9L xenograft. (B) Time–activity curve of ^{18}F-(2*S*,4*R*)4F-GLN in rats bearing 9L xenograft. Glutamine derivative displays prolonged tumor retention, whereas glutamic acid derivative shows faster washout. (C) Comparison of tumor-to-muscle ratio of ^{18}F-(2*S*,4*R*)4F-GLU and ^{18}F-(2*S*,4*R*)4F-GLN.

is associated with a high rate of glutaminolysis and a deregulated TCA cycle (*15,22*). Glutamine metabolism enables tumor cells to meet both the anaplerotic demands (forming intermediates of a metabolic pathway) and the energy demands of rapid growth. Transformed cells have a fast rate of glutamine consumption, and the rate of glutamine uptake can exceed 10 times what is required for protein and nucleotide synthesis. Glutamate can be converted to glutamine and thus functions as a substitute for glutamine, and its transamination product α-ketoglutarate is an important intermediate in the TCA cycle (*25*).

Radiolabeled ^{13}N-glutamine (^{13}N-GLN) and ^{13}N-glutamate (^{13}N-GLU) have been synthesized and evaluated (*33,34*). ^{13}N-GLN showed augmented uptake in malignant tumors and was evaluated clinically in patients having bone tumors. In a study comparing tumor uptake of ^{13}N-GLN and ^{13}N-GLU, ^{13}N-GLN showed a higher tumor uptake than ^{13}N-GLU in mouse xenografts. More recently, several ^{18}F-labeled glutamine and glutamate derivatives were developed and demonstrated promising results as tumor metabolic imaging agents (*23,25,26*). BAY 94-9392 showed an increased uptake in various tumors and had lower background uptake than ^{18}F-FDG. 4-^{18}F-fluoroglutamic acid (BAY 85-8050) exhibited rapid tumor uptake in lung and colon cancer cells (*25*). Because BAY 85-8050 is a diastereomeric mixture of ^{18}F-(2*S*,4*S*) and (2*S*,4*R*)-4-fluoro-glutamic acid, it complicates the analysis of biologic data. Recently, we developed a method for stereospecific synthesis of ^{18}F-(2*S*,4*R*)4F-GLN and showed its use as a tumor metabolic imaging agent. ^{18}F-(2*S*,4*R*)4F-GLN had a higher radiochemical yield and purity than corresponding (2*S*,4*S*) diastereomeric isomer (*23,24*). Hence, we focus on the comparative evaluation of ^{18}F-(2*S*,4*R*)4F-GLN and ^{18}F-(2*S*,4*R*)4F-GLU, which can provide insight on their utility as agents to image tumors and glutamine/glutamate metabolism in cancer cells.

It is not surprising that both in vitro and in vivo data showed that ^{18}F-(2*S*,4*R*)4F-GLN displayed a higher uptake than ^{18}F-(2*S*,4*R*)4F-GLU in tumor. The results suggested that several factors might contribute to the uptake of ^{18}F-(2*S*,4*R*)4F-GLN, including the upregulated system ASC (especially ASCT2 [*SLC1A5*]), increased protein synthesis, and glutaminolysis in tumor cells (*24*). In comparison, uptake of ^{18}F-(2*S*,4*R*)4F-GLU was due mostly to upregulation of system X_c^- (*SLC7A11*). A similar observation was reported previously by Koglin et al. (*26*). Increased uptake of amino acids and their close analogs in tumor cells may reflect upregulated amino acid transport activity or protein synthesis. Several clinically used amino acid tracers, such as ^{18}F-FET (*2*), *anti*-^{18}F-FACBC (*6*), and 3-^{123}I-iodo-L-α-methyl tyrosine (*35*), have increased uptake in cancer cells primarily resulting from upregulated system L transport activity. Several well-established amino acids, such as ^{11}C-methionine, ^{11}C-tyrosine, and 2-^{18}F-fluoro-L-tyrosine, are also involved in protein synthesis and other nonprotein metabolic pathways after transportation into cytosol. Although system L substrates have been the main focus for developing amino acid–based tracers in past decades and have achieved promising clinical results (*4,36*), new amino acid tracers targeting other deregulated transport systems in cancer cells could provide novel diagnostic and therapeutic tools. Transport activity of system X_c^- (*SLC7A11*), the cysteine/glutamate antiporter, has been shown in tumor cell lines including glioma, hepatoma, and head and neck cancer. System X_c^- (*SLC7A11*) is considered to be a potential target for cancer therapy (*26*). System ASC, in particular ASCT2 (*SLC1A5*), is overexpressed in numerous cancer cells and plays an essential role in tumor growth and survival (*32,37*). ASCT2 (*SLC1A5*) is regulated by c-Myc, whose overexpression is one of the most common alterations in human cancers (*21,38*). C-Myc regulates glutaminolysis as well and may lead to glutamine addiction in cancer cells, which is independent of Akt-directed aerobic glycolysis (*21*). Further studies to investigate the relationship between uptake of ^{18}F-(2*S*,4*R*)4F-GLN/^{18}F-(2*S*,4*R*)4F-GLU and overexpression of oncogene c-Myc and amino acid transport systems will be helpful in the evaluation and clinical application of these tracers (*23,24*).

One interesting observation is that the fluoride in ^{18}F-(2*S*,4*R*)4F-GLN did not have a considerable effect on its protein incorporation. However, ^{18}F-(2*S*,4*R*)4F-GLU was not incorporated into protein. Hence the uptake of ^{18}F-(2*S*,4*R*)4F-GLU was dominated by the increased transport activity. Although ASCT2 (*SLC1A5*) and X_c^- (*SLC7A11*) are both obligate amino acid exchangers (*32*), ASCT2 (*SLC1A5*) probably mediates mainly ^{18}F-(2*S*,4*R*)4F-GLN influx, because ^{18}F-(2*S*,4*R*)4F-GLN was quickly converted to other metabolites and thus could not be transported out via ASCT2 (*SLC1A5*). In contrast, since ^{18}F-(2*S*,4*R*)4F-GLU remained mostly in its parent form, it might efflux via X_c^- (*SLC7A11*). This might explain the difference in retention time in tumor cells between ^{18}F-(2*S*,4*R*)4F-GLN and ^{18}F-(2*S*,4*R*)4F-GLU. Despite the fact that uptake of ^{18}F-(2*S*,4*R*)4F-GLU was not as high as that of ^{18}F-(2*S*,4*R*)4F-GLN, the lower background of ^{18}F-(2*S*,4*R*)4F-GLU yielded a higher tumor-to-background ratio, which is a beneficial property for a tumor imaging agent. Brain uptake of ^{18}F-(2*S*,4*R*)4F-GLN and ^{18}F-(2*S*,4*R*)4F-GLU in biodistribution and small-animal PET studies was low, indicating that the newly developed ligands will not have easy access to regions of gliomas with relatively intact blood–brain barriers. Penetration of this barrier has been a major obstacle to using non–system L transport substrates for primary brain tumor imaging. It is evident that several competing factors, including tumor tissue uptake, in vivo defluorination, and background clearance, are important for defining the PET images. Further investigation into the metabolic fate of this tracer is undergoing investigation. Additionally, investigations to compare ^{18}F-(2*S*,4*R*)4F-GLN and ^{18}F-(2*S*,4*R*)4F-GLU with the new tracer BAY 94-9392 will be subject to further investigations.

Ultimately, optimal in vivo kinetics of tumor uptake versus background activity in patients will likely determine the potential utility of these two seemingly similar tumor imaging agents.

CONCLUSION

This paper presents the first, to our knowledge, comparison of ^{18}F-labeled enantiomerically pure glutamine and glutamate derivatives as tumor metabolic imaging agents. In vitro studies demonstrated that tumor cell uptake of ^{18}F-(2*S*,4*R*)4F-GLN was higher than that of ^{18}F-(2*S*,4*R*)4F-GLU, and this finding may be due to increased amino acid transport activity, protein incorporation, and nonprotein metabolic pathways such as glutaminolysis. In contrast, ^{18}F-(2*S*,4*R*)4F-GLU was not incorporated into protein, and therefore the uptake is predominantly controlled by the transporter. In vivo studies showed that ^{18}F-(2*S*,4*R*)4F-GLN exhibited a higher uptake and longer retention in rats bearing 9L tumor xenographs, whereas ^{18}F-(2*S*,4*R*)4F-GLU showed a slightly higher tumor-to-background ratio due to a faster background clearance. Both ^{18}F-(2*S*,4*R*)4F-GLN and ^{18}F-(2*S*,4*R*)4F-GLU may be potentially useful as tumor metabolic imaging agents.

DISCLOSURE STATEMENT

The costs of publication of this article were defrayed in part by the payment of page charges. Therefore, and solely to indicate this fact, this article is hereby marked "advertisement" in accordance with 18 USC section 1734.

ACKNOWLEDGMENTS

This work was supported in part by grants from Stand-Up 2 Cancer (SU2C) and the National Institutes of Health (CA-164490). No other potential conflict of interest relevant to this article was reported.

REFERENCES

1. Tanaka Y, Nariai T, Momose T, et al. Glioma surgery using a multimodal navigation system with integrated metabolic images. *J Neurosurg.* 2009;110:163–172.
2. Langen KJ, Hamacher K, Weckesser M, et al. O-(2-[^{18}F]fluoroethyl)-L-tyrosine: uptake mechanisms and clinical applications. *Nucl Med Biol.* 2006;33:287–294.
3. Kaira K, Oriuchi N, Shimizu K, et al. ^{18}F-FMT uptake seen within primary cancer on PET helps predict outcome of non-small cell lung cancer. *J Nucl Med.* 2009;50:1770–1776.
4. McConathy J, Goodman Mark M. Non-natural amino acids for tumor imaging using positron emission tomography and single photon emission computed tomography. *Cancer Metastasis Rev.* 2008;27:555–573.
5. McConathy J, Voll RJ, Yu W, Crowe RJ, Goodman MM. Improved synthesis of *anti*-[^{18}F]FACBC: improved preparation of labeling precursor and automated radiosynthesis. *Appl Radiat Isot.* 2003;58:657–666.
6. Yu W, Williams L, Camp V, Olson J, Goodman M. Synthesis and biological evaluation of *anti*-1-amino-2-[^{18}F]fluoro-cyclobutyl-1-carboxylic acid (*anti*-2-[^{18}F]FACBC) in rat 9L gliosarcoma. *Bioorg Med Chem Lett.* 2010;20:2140–2143.
7. Yu W, Williams L, Camp VM, Malveaux E, Olson JJ, Goodman MM. Stereoselective synthesis and biological evaluation of *syn*-1-amino-3-[^{18}F]fluorocyclobutyl-1-carboxylic acid as a potential positron emission tomography brain tumor imaging agent. *Bioorg Med Chem.* 2009;17:1982–1990.
8. Pöpperl G, Kreth FW, Herms J, et al. Analysis of ^{18}F-FET PET for grading of recurrent gliomas: is evaluation of uptake kinetics superior to standard methods? *J Nucl Med.* 2006;47:393–403.
9. Oka S, Hattori R, Kurosaki F, et al. A preliminary study of *anti*-1-amino-3-^{18}F-fluorocyclobutyl-1-carboxylic acid for the detection of prostate cancer. *J Nucl Med.* 2007;48:46–55.
10. Schuster DM, Savir-Baruch B, Nieh PT, et al. Detection of recurrent prostate carcinoma with *anti*-1-amino-3-^{18}F-fluorocyclobutane-1-carboxylic acid PET/CT and ^{111}In-capromab pendetide SPECT/CT. *Radiology.* 2011;259:852–861.
11. Okudaira H, Shikano N, Nishii R, et al. Putative transport mechanism and intracellular fate of *trans*-1-amino-3-^{18}F-fluorocyclobutanecarboxylic acid in human prostate cancer. *J Nucl Med.* 2011;52:822–829.
12. Dang CV. Rethinking the Warburg effect with Myc micromanaging glutamine metabolism. *Cancer Res.* 2010;70:859–862.
13. Albihn A, Johnsen J, Henriksson M. MYC in oncogenesis and as a target for cancer therapies. *Adv Cancer Res.* 2010;107:163–224.
14. Dang CV. Glutaminolysis: supplying carbon or nitrogen or both for cancer cells? *Cell Cycle.* 2010;9:3884–3886.
15. Dang CV, Hamaker M, Sun P, Le A, Gao P. Therapeutic targeting of cancer cell metabolism. *J Mol Med.* 2011;89:205–212.
16. Wellen KE, Thompson CB. Cellular metabolic stress: considering how cells respond to nutrient excess. *Mol Cell.* 2010;40:323–332.
17. Gao P, Tchernyshyov I, Chang T, et al. c-Myc suppression of miR-23a/b enhances mitochondrial glutaminase expression and glutamine metabolism. *Nature.* 2009;458:762–765.
18. Thompson CB. Metabolic enzymes as oncogenes or tumor suppressors. *N Engl J Med.* 2009;360:813–815.
19. Cheng T, Sudderth J, Yang C, et al. Pyruvate carboxylase is required for glutamine-independent growth of tumor cells. *Proc Natl Acad Sci U S A.* 2011;108:8674–8679.
20. Rajagopalan KN, Deberardinis RJ. Role of glutamine in cancer: therapeutic and imaging implications. *J Nucl Med.* 2011;52:1005–1008.
21. Wise DR, DeBerardinis R, Mancuso A, et al. Myc regulates a transcriptional program that stimulates mitochondrial glutaminolysis and leads to glutamine addiction. *Proc Natl Acad Sci U S A.* 2008;105:18782–18787.

22. Shanware NP, Mullen AR, DeBerardinis RJ, Abraham RT. Glutamine: pleiotropic roles in tumor growth and stress resistance. *J Mol Med.* 2011;89:229–236.
23. Qu W, Zha Z, Ploessl K, et al. Synthesis of optically pure 4-fluoro-glutamines as potential metabolic imaging agents for tumors. *J Am Chem Soc.* 2011;133:1122–1133.
24. Lieberman BP, Ploessl K, Wang L, et al. PET imaging of glutaminolysis in tumors by ^{18}F-(2*S*,4*R*)4-fluoroglutamine. *J Nucl Med.* 2011;52:1947–1955.
25. Krasikova RN, Kuznetsova OF, Fedorova OS, et al. 4-[^{18}F]-fluoroglutamic acid (BAY 85-8050), a new amino acid radiotracer for PET imaging of tumors: synthesis and in vitro characterization. *J Med Chem.* 2011;54:406–410.
26. Koglin N, Mueller A, Berndt M, et al. Specific PET imaging of xC- transporter activity using a ^{18}F-labeled glutamate derivative reveals a dominant pathway in tumor metabolism. *Clin Cancer Res.* 2011;17:6000–6011.
27. Lindholm P, Minn H, Leskinen-Kallio S, Bergman J, Ruotsalainen U, Joensuu H. Influence of the blood glucose concentration on FDG uptake in cancer: a PET study. *J Nucl Med.* 1993;34:1–6.
28. Nakanishi T, Sugawara M, Huang W, et al. Structure, function, and tissue expression pattern of human SN2, a subtype of the amino acid transport system N. *Biochem Biophys Res Commun.* 2001;281:1343–1348.
29. Gout PW, Buckley AR, Simms CR, Bruchovsky N. Sulfasalazine, a potent suppressor of lymphoma growth by inhibition of the x(c)- cystine transporter: a new action for an old drug. *Leukemia.* 2001;15:1633–1640.
30. Kansal VK, Sharma R, Rehan G. Characterization of anionic amino acid transport systems in mouse mammary gland. *Indian J Exp Biol.* 2000;38:1097–1103.
31. Gambhir SS. Molecular imaging of cancer: from molecules to humans—introduction. *J Nucl Med.* 2008;49(suppl 2):1S–4S.
32. Ganapathy V, Thangaraju M, Prasad P. Nutrient transporters in cancer: relevance to Warburg hypothesis and beyond. *Pharmacol Ther.* 2009;121:29–40.
33. Conlon KC, Bading JR, DiResta GR, Corbally MT, Gelbard AS, Brennan MF. Validation of transport measurements in skeletal muscle with N-13 amino acids using a rabbit isolated hindlimb model. *Life Sci.* 1989;44:847–859.
34. Gelbard AS, Christie TR, Clarke LP, Laughlin JS. Imaging of spontaneous canine tumours with ammonia and L-glutamine labeled with N-13. *J Nucl Med.* 1977;18:718–723.
35. Pauleit D, Floeth F, Tellmann L, et al. Comparison of O-(2-^{18}F-fluoroethyl)-L-tyrosine PET and 3-^{123}I-iodo-alpha-methyl-L-tyrosine SPECT in brain tumors. *J Nucl Med.* 2004;45:374–381.
36. Jager PL, Vaalburg W, Pruim J, de Vries EG, Langen KJ, Piers DA. Radiolabeled amino acids: basic aspects and clinical applications in oncology. *J Nucl Med.* 2001;42:432–445.
37. Fuchs BC, Bode BP. Amino acid transporters ASCT2 and LAT1 in cancer: partners in crime? *Semin Cancer Biol.* 2005;15:254–266.
38. Dang CV, Le A, Gao P. MYC-induced cancer cell energy metabolism and therapeutic opportunities. *Clin Cancer Res.* 2009;15:6479–6483.

JNM The Journal of NUCLEAR MEDICINE

Comparative Evaluation of ^{18}F-Labeled Glutamic Acid and Glutamine as Tumor Metabolic Imaging Agents

Karl Ploessl, Limin Wang, Brian P. Lieberman, Wenchao Qu and Hank F. Kung

J Nucl Med. 2012;53:1616-1624.
Published online: August 30, 2012.
Doi: 10.2967/jnumed.111.101279

The Journal of Nuclear Medicine is published monthly.
SNMMI | Society of Nuclear Medicine and Molecular Imaging
1850 Samuel Morse Drive, Reston, VA 20190.
(Print ISSN: 0161-5505, Online ISSN: 2159-662X)

SNMMI SOCIETY OF NUCLEAR MEDICINE AND MOLECULAR IMAGING